Reconfigurable Soft Flexure Hinges via Pinched Tubes

Yuhao Jiang[1†], Mohammad Sharifzadeh[2†], Daniel M. Aukes[2*]

Abstract— **Tuning the stiffness of soft robots is essential in order to extend usability and control the maneuverability of soft robots. In this paper, we propose a novel mechanism that can reconfigure the stiffness of tubular structures, using pinching to induce highly directional changes in stiffness. When pinched, these tubes can be then utilized as flexure hinges to create virtual joints on demand; the orientation of the hinge axis can additionally be selected via control of the distribution of pinch forces on the surface of the tube. Through proper material and geometry selection, passive shape recovery is observed when pinching forces are removed; a proposed active shape recovery technique can further assist the tube to recover its initial shape in order to re-configure the hinge in a new orientation. The proposed mechanism has been validated in FEA as well as experimentally, looking specifically at the relation between pinching force and curvature change, as well as comparing tube stiffness between pinched and unpinched configurations. The experimental prototype detailed in this paper – and demonstrated in the associated video – is capable of controlling the generation and recovery of flexure hinges at multiple orientations around the radial axis of tubes on demand.**

I. INTRODUCTION

The purpose of this paper is to demonstrate how thin-walled cylindrical tubes can be pinched to create compliant, virtual joints in any radial direction, and then recover their original shape and stiffness once released. Through careful design and material selection, this can result in large changes in stiffness between the original shape, the intended degree of freedom, and orthogonal axes; resulting flexures can then used as passive, compliant rotational joints.

This work is motivated by soft robots, which have received attention in recent years due to their ability to interact with the world in complex ways using simple, continuously deformable structures made with soft materials [1]. Such robots often emulate bio-inspired systems such as snakes [2]–[6], octopuses [7]–[10], and elephant trunks [11]–[13] due to their ability to contort themselves into highly complex shapes that would ordinarily be impossible with traditional rigid robots. This is possible because local curvature in any direction can be induced through the proper mixing of internal actuator forces. However, because of the material-dependent nature of soft-bodied robots, control difficulties can arise due to the high computational cost of estimating pose and

[1]School for Engineering of Matter, Transport and Energy, Fulton Schools of Engineering, Arizona State University, Tempe, AZ, 85281, USA `yuhao92@asu.edu`

[2]The Polytechnic School, Fulton Schools of Engineering, Arizona State University, Mesa, AZ, 85212, USA

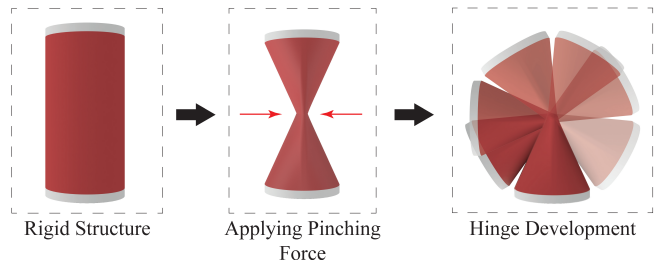[*]Address all correspondence to this author. `danaukes@asu.edu`

Fig. 1. Conceptual rendering of the proposed mechanism. A cylindrical tube is deformed by pinching, resulting in a flexure hinge that can rotate when a load is applied at the end.

optimizing trajectory in redundant, high degree-of-freedom, continuum robots. In order to ameliorate these difficulties while utilizing the natural deformability of soft robots, a great deal of research has looked into tuning the stiffness of soft robots for the purpose of simplifying models and making more efficient controllers [14], including utilizing jamming [15], [16], active elastomers [17], tendon-driven solutions [18], as well as anisotropic [19] and functionally graded materials [20].

Tuning the shape or curvature of soft devices has been studied for its ability to alter system stiffness. Nguyen et al. highlight how curvature-change can modulate the stiffness of fish fins [21], while Pini et al. detail how internal stress fields can impart stiffness changes in thin sheets via two-dimensional bending [22]. This can be enhanced by weakening or creasing material along a curve to produce rapid transitions between static states in curved soft materials [23]. Curvature and shape change may also be actively controlled for the purposes of changing stiffness [24]. Some compact examples include the use of SMA tendons [25] and springs [26].

Across the various research which has been performed in this area, the majority focuses on how the design and placement of internal actuation within continuum manipulators impacts arm state and end effector configuration via multiple actuators [2]–[13], [27]. Altering stiffness has previously been accomplished through numerous approaches [14]–[20], but within the body of work focusing on curvature-influenced stiffness, papers focus on mechanics or stability analysis [21]–[23] while others use one degree of actuation to stiffen or soften a geometry [24]–[26]. In contrast with these studies, this work investigates how combining the forces of more than one actuator can influence the creation and orientation of flexure hinges in tubes, and how, with proper geometry and material selection, those hinges can then passively or actively revert back to a stiffer tubular struc-

ture. These devices, if properly implemented in continuum devices, could permit soft robots to utilize simpler models akin to their rigid counterparts while retaining the benefits of soft robots.

In order to realize this concept, we propose to change the local surface curvature of thin-walled tubes in order to alter local bending stiffness; in this way local buckling makes the tube's altered mechanical properties suitable for use as a flexure hinge about the buckled region. We believe this novel soft hinge, shown in Fig.1, fits within a larger class of kinematic elements which we call Soft, Curved, Reconfigurable, Anisotropic Mechanisms, or SCRAMs. Like the bio-inspired mechanisms mentioned above, SCRAMs are capable of re-configuring the stiffness of curved surfaces for use as virtual joints in soft robots. The proposed SCRAM mechanism in this paper re-configures its internal stiffness through the application of opposed pairs of pinching forces (via actuated pairs of tendons) on the surface of the tube. By controlling the distribution of forces exerted through the tendons, this SCRAM device is able to flatten the tube in different radial orientations, permitting one to select the hinge's axis of rotation on demand. In doing so, the concept proposed in this paper extends prior work mentioned above, enhancing the usability of stiffness tuning mechanisms for more complex applications such as robotic arms and snake-like robots. Furthermore, in contrast to prior work, which uses shape change in soft systems directly for actuation purposes, our approach uses shape change and reconfiguration indirectly, for the purpose of reducing system stiffness about a desired hinge axis. Actuator forces are directed orthogonal to system outputs, minimizing their contribution to work done at the end effector – an advantage for sizing future shape change actuators, which we discuss in the conclusion.

In the following sections, we discuss the principle of operation for the proposed mechanism, using finite element analysis (FEA) to understand the relationship between distributed pinching forces, curvature, and system stiffness. We then propose a set of criteria to evaluate the performance of the mechanism and experimentally validate the concept with a benchtop prototype. We then analyze and compare the stiffness change between pinched and unpinched tubes, and provide insights as to the impact of our work and future research directions.

II. FEA Modeling

In this section, we validate the efficacy of the proposed mechanism by conducting a Finite Element Analysis (FEA) study on a cylindrical tube with 0.1 m radius, 0.3 m length, 0.001 m wall thickness and 2.96 GPa stiffness. Using FEA, we seek to demonstrate that a pair of opposing collinear forces exerted on a tube results in a highly deformed section of the tube's body and significantly lowers stiffness in comparison with an undeformed tube. In addition, we study the ability of a finite number of pinching forces to orient the major axis of deformation through 360°. Finally, we analyze the behavior of the pinched tube under various loading conditions.

The analysis is performed using SolidWorks Simulation; small modifications have been made to the tubular geometry in order to better localize constraints and force application points. In order to constrain the tube's circular cross-section at its proximal and distal ends, two rigid prismatic parts are merged with the tube's geometry. In order to provide pinching sites on the surface of the tube, small prismatic geometries are added to the interior of the tube halfway along its length. Fillets are used to transition between geometries to avoid part failure in these particular regions. The resulting geometry can be seen in Fig. 2(a).

The first analysis uses a nonlinear, static approach to model the interaction between pinching forces and tubular deformation. The mesh is created with 'Curvature-based mesh' elements with a minimum and maximum sizes of 2.7 mm and 8.1 mm, respectively, resulting in around 30200 nodes in the model. Our approach begins by determining the force required to completely pinch a tube until its sidewalls(or the added prismatic geometries) touch. This results in a weak section in the tube body (that is more conducive to bending like a flexure hinge). Figures in red, blue, and green circles in Fig. 2(d) show one pair of pinching forces deforming a tube till its interiors meet. This confirms the possibility of producing a nearly flat section in the tube while meeting the experimental result in Fig. 5(b).

When a pair of equal and opposite collinear pinch forces are applied to each side of the tube, the maximum deformation falls along a line that is orthogonal to the pinch force vectors (Figures with red, blue, and green circles in Fig. 2(d)) and the radial axis of the tube. We hypothesize that by combining multiple sets of force pairs, the orientation of this axis can thus be controlled to influence the resulting hinge orientation. Thus, our model has been augmented with multiple pairs of pinching forces, separated by an angular spacing θ of

$$\theta = \frac{360}{2n} \tag{1}$$

where n is the number of pinching unit pairs embedded in the tube.

Based on the above design assumptions, with two perpendicular unit pairs of pinching forces ($\theta = 90°$), our FEA reveals that the simultaneous actuation of the units, even at different force levels, does not result in a roughly elliptical cross section with a single major axis. Rather, the pinching forces create the dimpled-looking deformation seen in Fig. 2(b), with two independent, simultaneous perpendicular sets of major and minor deformation axes that we liken to a singularity consisting of multiple solutions.

A mechanism with three pairs of pinching units is subsequently studied. In this design $\theta = 60°$. The result, seen in Fig. 2(c), shows that simultaneous actuation of all three pairs at the same force magnitude results in the same dimpling as in the case of $n = 2$, with no clear major axis of deformation. Actuating only two of the pairs at a time, however, results in the tube deforming without multiple simultaneous solutions, which looks like the results for the case of a single pair of pinch forces.
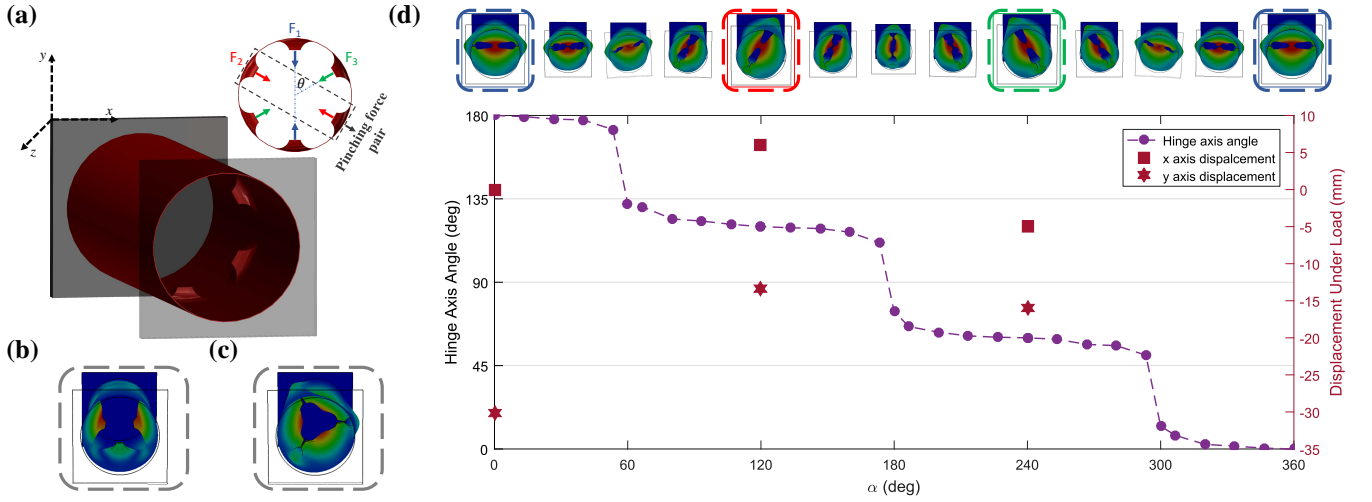
Fig. 2. **Finite element analysis on a pinched tube.** (a) The tube design in SolidWorks with inset of the cross-section at the midpoint. (b-c) Some tendon configurations fail to create a hinge, including (b) two pairs of pinch forces ($\theta = 90°$) and (c) three pairs of equivalent, radially symmetric pinch forces ($\theta = 60$). (d) FEA results showing the change in the hinge axis for different combinations of pinch forces as well as the displacement of the end effector when the tube is first pinched and load is subsequently applied.

In order to further study the effect of pinching forces on the tube's deformation axis, we define the following formulation for defining individual pinching forces:

$$F_{i1} = F_{i2} = F_p \cos(\beta) \tag{2}$$

$$F_{j1} = F_{j2} = F_p \sin(\beta) \tag{3}$$

$$F_{k1} = F_{k2} = 0 \tag{4}$$

where $i, j,$ and k correspond to the index of a pair of pinch forces, and F_p, and β relates to the magnitude of the force required to flatten the tube and pinch force distribution angle, respectively. Using the above equations, we separate the overall magnitude of the pinching force from its angle throughout the study. This allows us to focus on its direction change as function of β. We then introduce α to parameterize the change in pinch force pairs and the force distribution throughout 360°:

$$\beta = \begin{cases} 0.75\alpha & \text{for} & 0° \leq \alpha < 120° \\ 0.75(\alpha - 120°) & \text{for} & 120° \leq \alpha < 240° \\ 0.75(\alpha - 240°) & \text{for} & 240° \leq \alpha < 360° \end{cases} \tag{5}$$

$$(i, j, k) = \begin{cases} (1,2,3) & \text{for} & 0° \leq \alpha < 120° \\ (2,3,1) & \text{for} & 120° \leq \alpha < 240° \\ (3,1,2) & \text{for} & 240° \leq \alpha < 360° \end{cases} \tag{6}$$

The radar plot in figure 2(d) demonstrates how the major deformation axis can be affected through proper distribution of tension across the three tendon pairs. The inset renderings around the outside of the radar plot show the tube's deformation as a function of α. At $\alpha = 0°, 120°, 240°$, tendon tension F_p is concentrated on just one tendon (blue, red, and green, respectively), and for all other values of α, the tension is shared between tendon pairs i and j. The resulting axis angle can also be seen to increase monotonically as a function of α (violet circles in the interior radar plot), though rapid transitions can be found around $\alpha = 60°, 180°,$ and $300°$. At

these three values of α, F_p had to be increased by 50% in order to fully pinch the tube. We believe that this is caused by errors in the numerical solution at these particular values, potentially due to the geometries added to aid simulation. Future work will help to clarify this result as discussed in the conclusions.

Once the tube is deformed, FEA can also be used to study the flexure hinge's behavior under load. This is done by performing a nonlinear dynamics study. In this study the pinching forces are initially applied as before; once the tube deforms, a load is subsequently applied in the negative y direction to the top surface of the prismatic geometry attached to the distal end of the tube. The displacement of the prismatic block attached to the distal end of the tube in x and y axes are reported in Fig. 2(d) using squares and stars, respectively, for $\alpha = 0°, 120°, 240°$. For $\alpha = 0°$ (a horizontal hinge axis), the x displacement is zero and y displacement is maximized. For values where the loading direction is not orthogonal to the hinge axis, the displacement of the distal end of the tube qualitatively corresponds to the orthogonal of the resulting hinge axis vector (as seen in the attached video).

III. PROTOTYPING

A. Material Selection

This section provides details about the fabrication of experimental prototypes used to validate the concept described in the previous section. The suitability of each prototype is evaluated by a set of three criteria: (1) the force required to pinch the tube, (2) the ratio of radial stiffness anisotropy at the flexure hinge, and (3) the ability of the tube to recover its original shape without plastic deformation after forces are removed. Since the proposed mechanism is eventually intended to be used for mobile robotic applications, the servo selected for prototyping and experimentation was small, with

a stall torque of 4 Nm, constraining the maximum pinch force we could use to deform prototype tubes. While it would be desirable to select designs that simply minimize the force required to create local deformation (criteria 1), the use of softer materials or thinner cylinder walls could lead to failure of the second criteria, which considers the ability of the flattened tube to act like a flexure hinge; this is an essential characteristic of our proposed mechanism so that hinges flex when loaded about the hinge axis yet remain stiff to orthogonal loads. The higher the stiffness ratio between these two directions, the better the hinge. The third criteria considers the ability of a design to passively recover its tubular shape without damage – essential if this mechanism is to be used repetitively in the context of robotics applications. We know from basic mechanics principles as well as texts like [28] that thinner cylinder walls, larger diameters and lower Young's modulus will lower system stiffness and permit easier pinching, but will also limit the maximum stiffness of the system for resisting deformation in unintended directions.

We selected a number of different cylindrical tubes made from thermoplastic polyurethane (TPU), polyethylene terephthalate (PET), and latex rubber (Shore hardness 35A). Looking first at the latex rubber tube, a number of drawbacks can be observed. Although it can be deformed by a pinch force of 10 N (criteria 1) and is good at recovering its shape without damage (criteria 3), the flexure hinge created when the tube is pinched exhibits little difference in stiffness when bent in its intended orientation and a direction orthogonal to it. This is due to the thick cylinder wall needed to sufficiently stiffen the tube, indicating that the Young's modulus of the latex rubber makes it unusable for this particular SCRAM device, as it functions poorly as a simple joint (criteria 2).

PET on the other hand, is a semi-rigid, elastic material widely used for soda and water bottles; at 180 mm length, 72 mm diameter and 1 mm wall thickness, it can be deformed into a pinched tube while maintaining the ability to sustain a high degree of rigidity in directions orthogonal to pinching while easily rotating about its flexure hinge (criteria 2). An example of this tube is shown in Fig. 3(a). However, a number of drawbacks were observed while testing the PET tube. First, the force required to pinch the material is relatively large, which violates criteria 1. Moreover, due to the nature of the PET, some scars were created on the tube's surface which were visible after recovery, indicating high stresses had plastically deformed the material during its use as a joint, violating criteria 3. Furthermore, as shown in Fig. 3(b), the PET tube did not passively recover its shape, but required an external force to initiate recovery. While a thinner cylinder wall would reduce stiffness and potentially lower the local stresses that led to that plastic deformation, samples in the desired dimensions were not readily available; for these reasons the PET tube was abandoned as a suitable alternative.

TPU possesses high elasticity and high sheer strength properties, and has been broadly used in fabricating soft robots [29], [30]. In terms of its suitability as a SCRAM
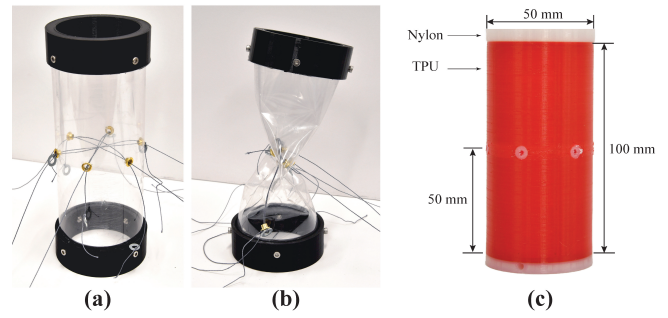

Fig. 3. **Prototypes made from different materials. (a):** PET prototype. **(b):** PET prototype after deformation. **(c):** TPU prototype specifications.
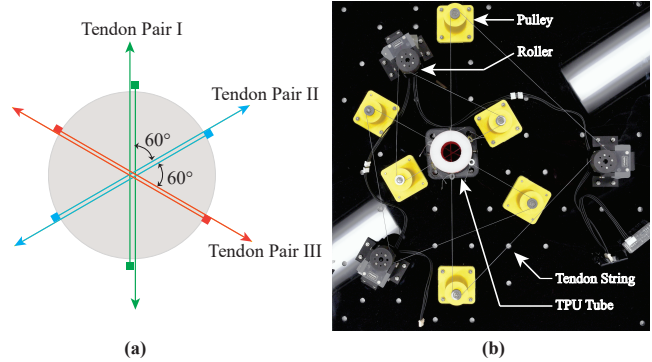

Fig. 4. **Test setup and tendon configuration. (a):** Tendon string orientation. **(b):** Prototype with servos and pulleys.

hinge, the pinching force required to deform TPU is lower than PET (criteria1). When pinched, the TPU tube exhibits high compliance in the intended direction of hinge motion compared to a relatively stiff behavior in other directions, making it highly suitable with regard to criteria 2. In terms of recovery, the high elasticity of TPU also permits full, unaided recovery from its flattened state without any visible scarring (criteria 3). Additionally, because it is compatible with 3D printing processes, its shape can be adjusted and reprinted as more is learned about its performance. Owing to these merits, TPU was adopted as the material for subsequent prototypes and experiments.

B. Prototyping

The main body of the current prototype, shown in Fig.3(c), is 3D printed from TPU92A[1] with an Ultimaker S5. The geometry of the tube (100 mm long, 50 mm diameter and 1 mm wall thickness)was primarily constrained by the printing capability of our printer, the size of our testbed, and the force limits of the tendon-driven actuation system. Though this geometry was not optimized against a set of quantitative performance criteria, it was observed to qualitatively satisfy each of our stated criteria within the limitations of available materials, printing, and testing capabilities. Two rigid nylon attachment plates were co-printed to the bottom and the top of the cylinder, and six round metal grommets were

[1]produced by Ultimaker [31]

radially distributed around the length midpoint of the body so that tendons could pass through the tube without cutting or abrading the material.

In order to show the potential for controlling the orientation of the resulting soft flexure hinge, this prototype is actuated using a tendon-based system to impart three separate pinching forces around the circumference of the tube. Six tendons are routed individually through one of the grommets and then routed and connected to one of three Dynamixel XM430-W350-T servos through a system of pulleys attached to ground, making it possible to symmetrically drive a pair of tendons from one servo so that three equal and opposite pairs of pinch forces may be individually applied to the tube at $60°$ radial spacing, matching the arrangement of the FEA simulation. The tendon distribution and the final test setup may be seen in Fig. 4(a) and (b) respectively. The pinching force and the amount of tube deformation are measured by the torque and the position of the servo.

IV. PINCHING FORCE VS. TUBE CURVATURE

The relationship between pinching force and tube curvature is discussed next. We approach the problem both to understand the relationship between pinching force magnitude and the amount of deformation, as well as to understand the relationship between the distribution of pinch forces across the tendons and the resulting flexure hinge's orientation.

A. Pinching Force V.S. Deformation

To understand the relationship between pinching force and tube deformation, we have measured tendon force at sample positions via Dynamixel servos. This test has been conducted with the servos operating in position control mode, wherein the servo's embedded controller applies a control signal to drive the servo to a goal position, which is tracked internally. By actuating the servo to pull the tendon a certain length, the surface of the tube correspondingly deforms.

In our test, the servo starts from a position corresponding to a fully undeformed tube, and increments by a small amount until the final tendon displacement equals the radius of the tube. The servos' position and current are recorded at each increment. Tendon tension is then calculated by recording the motor current at each step and calculating the tendon forces as a function of both the current/torque curve provided by the manufacturer [32] and the radius of the output pulley. Because each tendon is routed through a minimum number of pulleys, we assume that the majority of the current applied by each motor is transmitted into a pinching force rather than lost within the tendon system itself. The relationship between pinching force and the tube's deformation can be seen in Fig. 5(a). By controlling the magnitude of the pinching force, a specific amount of deformation can be established in the tube that is qualitatively consistent with our FEA results.

B. Orientation of the Pinching Force V.S. Deformation Direction

To understand the relationship between the orientation of the pinching force and the direction of the deformation, we conducted another set of experiments, pulling different tendons aligned along different orientations in order to generate pinching forces in different directions. This was accomplished by commanding the servo (in position control mode) to pull the tendon so that appropriate pinch forces were generated to deform the structure, similar to the FEA analysis discussed in Section II. As can be seen in Fig 5(b), the orientation of the flexure hinge changed as a function of tendon force distribution. This result also qualitatively matches with the results seen in Fig. 2(d) and discussed in Section II.

Based on the aforementioned tests, the relationship between the pinching force and the curvature generation can be better understood. The magnitude of the pinching force is positively correlated to the flattening of the tubular structure, and the direction of the curvature depends on the orientation of the pinching force.

V. EVALUATION OF THE FLEXURE HINGE

In this section, we evaluate the performance of the flexure hinge generated by pinching, examining joint stiffness as well as its directional displacement when loaded with with forces in varying directions.

A. Bending Stiffness Analysis

This section deals with changes in tube stiffness due to pinching. The experimental setup is shown in Fig. 6(a). In this test, a linear stage pushes a contact point parallel to the ground while an ATI Mini40 six-axis force-torque sensor records the forces. This was conducted over multiple trials for different displacements in both the pinched and unpinched configuration, as shown in Fig. 6(b). To better understand the difference in stiffness due to pinching, we compare the slopes of the linear regions between the pinched and unpinched states. As shown by the slopes of each linear fit, as seen in Fig. 6(b), the difference between pinched and unpinched configurations results in a dramatic stiffness change from $k_1 = 1812\,N/m$ to $k_2 = 148.6\,N/m$; in other words, the stiffness of the unpinched tube is 12 times stiffer than the pinched tube.

Figure 6 also shows that the load increases linearly as a function of forward displacement in both the pinched and unpinched configuration. Linear behavior can also be observed when moving backward, though hysteresis is present. It can be seen that the pinched configuration exhibits much more hysteresis, which we can attribute to several factors. First, because the displacements for the pinched experiment are generally larger, viscoelastic creep due to our material selection may be amplified and more noticeable. As discussed previously, TPU has been selected for its ability to recover without noticeable plastic deformation, but it may not be an ideal material in other ways. Hysteresis may also be caused by the fact that the inner surfaces of the tube may slide against each other when the system is fully pinched, which can lead to frictional losses and a new static equilibrium after bending. This is supported by the fact that after larger displacements, the tube did not fully recover while still in
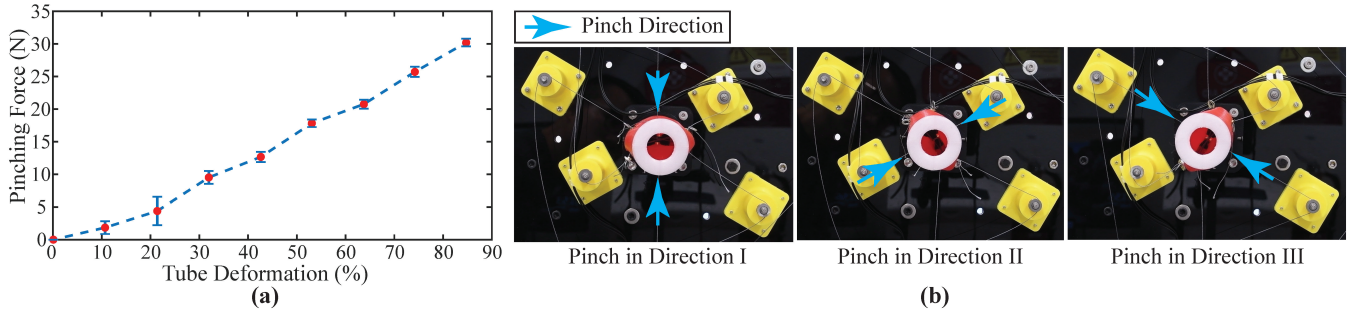
Fig. 5. **Pinch force and the corresponding deformation. (a):** Pinch force required to reach specific tube deformation. **(b):** Pinch in three different directions with 60° radial spacing and the hinge developed correspondingly.

its pinched state; After tendon tension was relaxed and the tube recovered its initial shape, however, its performance when pinched again exhibited the same linear behavior across repeated tests.
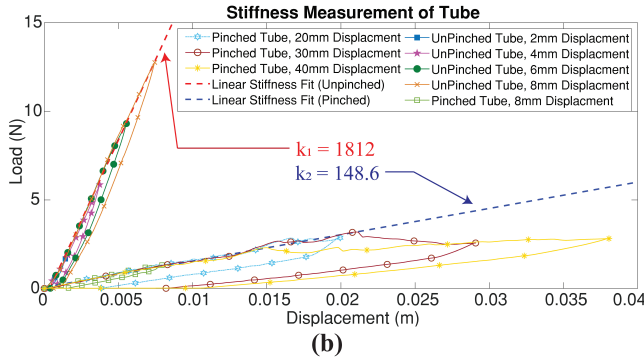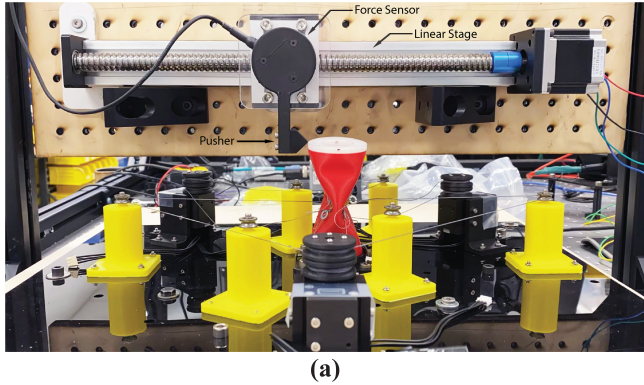

Fig. 6. **Bending Stiffness Analysis. (a):** Test setup including linear stage, force sensor, and pusher. **(b):** Bending Stiffness comparison for pinched and unpinched tube.

B. Alignment of Forces, Hinge Axes, and Resulting Displacements

To validate the suitability of the flexure hing to perform as a revolute joint, we orient the test setup so that the tube's radial axis is perpendicular to the ground. A 500 g weight is attached to the end of the structure. The servo is then commanded in velocity mode to fully pinch the tube at a constant speed. The tendons parallel with the gravity vector are actuated in the first example, so that the resulting

flexure hinge is perpendicular to the gravity vector. In order to eliminate the effect of the unpinched tendons, the other servos are driven so as to keep those tendons slack.

During this test we observe that as the tendon force increases, the tube's curvature changes, and the structure gets visibly weaker until it buckles, demonstrating a drastic change in stiffness around a newly created hinge. This procedure is shown in the supplementary video.

Two other tests have been conducted to demonstrate that the hinges generated using this concept behave similarly to a formal revolute joint, which is commonly used in robotics to provide rotation about a single-axis. In these two tests, we actuate the other two pairs of the tendon individually so that the pinching force is applied in two different directions at an angle of $\pm 60°$ relative to gravity. As before, a load of 500 g is attached to the end of the structure and the servos are commanded to to pinch the tube at a constant speed. As can be seen in Fig.7(a), the structure deforms as the tendon is pulled to its limit. Since the orientation of the resulting hinge varies, the direction of the end-effector's motion about the hinge axis changes concurrently in response to the same load.

VI. SHAPE RECOVERY OF THE FLEXURE HINGE

As an essential part of hinge reconfiguration, we study the recovery of the flattened tube back to its circular cross-section. During the tests introduced in Section V.A, we found that the tube was able to passively recover its shape under 500 g load when the pinching force was removed. This is due to the stiffness, geometry, and the elastic nature of TPU. This result also validates the shape recovery requirement of our selection criteria.

The tube was also evaluated at a load of 1000 g. In this case, the TPU was unable to passively recover without aid. Instead, an active strategy was used. The two tendons exerting pinching forces were first released and the other two pairs of pinch tendons were lightly actuated to pinch the tube antagonistically in other two directions. This resulted in the tube regaining its tubular shape under load, as can be seen in Fig. 7(b), as well as in the supplementary video.

VII. CONCLUSIONS AND FUTURE WORK

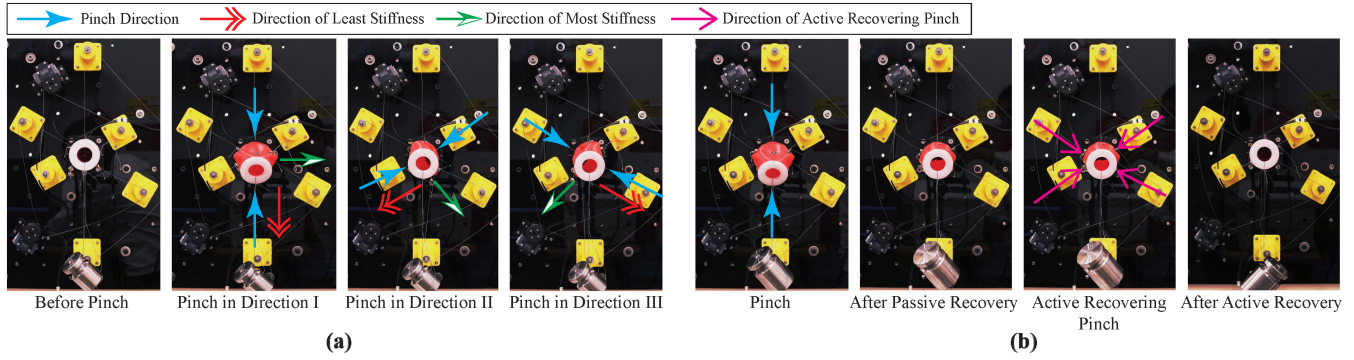This paper introduces a novel concept for tuning the stiffness of a thin-walled tube by altering the local sur-

| Pinch Direction | Direction of Least Stiffness | Direction of Most Stiffness | Direction of Active Recovering Pinch |

| Before Pinch | Pinch in Direction I | Pinch in Direction II | Pinch in Direction III |
(a)

| Pinch | After Passive Recovery | Active Recovering Pinch | After Active Recovery |
(b)

Fig. 7. **Creation of flexure hinges and subsequent recovery. (a):** Deformation of tubes under 500 g load with differing hinge orientations. **(b):** Recovery of tubular shape (under 1000 g load) using active and passive approaches.

face curvature through pinching. Its intellectual contributions include (i) a physical implementation of this concept, (ii) understanding and evaluation of the relationship between the pinching force and the tube deformation supplied both by FEA and experiment; (iii) insights into how the combination of multiple pinching forces can be used to orient the major axis of deformation and resulting flexure hinge, demonstrated in FEA and experiment (iv) experimental evaluation of the suitability of the resulting hinge for use as a joint including its stiffness and displacement under load, and (v) prototype-based validation of active and passive shape recovery of the tube.

Future work will mainly focus on actuation, sensing, and applications of the proposed concept. To begin with, a better normalization of our FEA model will permit a more uniform distribution of tendon forces to increase consistency of deformation and hinge performance throughout 360°. This will lead to a better understanding of how our design parameters can improve system performance in order to use multiple hinges as a system. Our aim is to permit more complex, reconfigurable mechanisms such as robot arms and snake-inspired designs. We will also look into ways to improve the systems for pinching and actuating the hinge. As can be seen in Section III B, although the tendon based actuating system used in the test setup can effectively pinch the tube and verify the principle of operation, in its current state is too complex and bulky for applications outside of an experimental test bed, if we wish to integrate multiple SCRAM stages together, for example. This drawback motivates us to search for and develop more portable and simpler actuating systems that can effectively pinch and actuate the hinge. We believe our approach of actuating internal shape and stiffness change (rather than end-effector motion), in conjunction with additional materials and geometry optimization, will eventually permit lower-power and more compact actuators to be integrated within the tubular system itself. New methods to sense local deformation will also be necessary in order to close the loop and actively control shape change in future SCRAM devices.

REFERENCES

[1] D. Rus and M. T. Tolley, "Design, fabrication and control of soft robots," *Nature*, vol. 521, no. 7553, pp. 467–475, 2015.

[2] C. D. Onal and D. Rus, "Autonomous undulatory serpentine locomotion utilizing body dynamics of a fluidic soft robot," *Bioinspiration and Biomimetics*, vol. 8, no. 2, 2013.

[3] R. F. Shepherd, F. Ilievski, W. Choi, S. A. Morin, A. A. Stokes, A. D. Mazzeo, X. Chen, M. Wang, and G. M. Whitesides, "Multigait soft robot," *Proceedings of the National Academy of Sciences of the United States of America*, vol. 108, no. 51, pp. 20 400–20 403, 2011.

[4] M. Luo, W. Tao, F. Chen, T. K. Khuu, S. Ozel, and C. D. Onal, "Design improvements and dynamic characterization on fluidic elastomer actuators for a soft robotic snake," *IEEE Conference on Technologies for Practical Robot Applications, TePRA*, pp. 1–6, 2014.

[5] H. Marvi and D. L. Hu, "Friction enhancement in concertina locomotion of snakes," *Journal of the Royal Society Interface*, vol. 9, no. 76, pp. 3067–3080, 2012.

[6] F. Renda, M. Giorelli, M. Calisti, M. Cianchetti, and C. Laschi, "Dynamic model of a multibending soft robot arm driven by cables," *IEEE Transactions on Robotics*, vol. 30, no. 5, pp. 1109–1122, 2014.

[7] M. Calisti, M. Giorelli, G. Levy, B. Mazzolai, B. Hochner, C. Laschi, and P. Dario, "An octopus-bioinspired solution to movement and manipulation for soft robots," *Bioinspiration and Biomimetics*, vol. 6, no. 3, 2011.

[8] C. Laschi, M. Cianchetti, B. Mazzolai, L. Margheri, M. Follador, and P. Dario, "Soft robot arm inspired by the octopus," *Advanced Robotics*, vol. 26, no. 7, pp. 709–727, 2012.

[9] L. Margheri, B. Mazzolai, M. Cianchetti, P. Dario, and C. Laschi, "Tools and methods for experimental in-vivo measurement and biomechanical characterization of an Octopus vulgaris arm," *Proceedings of the 31st Annual International Conference of the IEEE Engineering in Medicine and Biology Society: Engineering the Future of Biomedicine, EMBC 2009*, pp. 7196–7199, 2009.

[10] G. Sumbre, G. Fiorito, T. Flash, and B. Hochner, "Octopuses Use a Human-like Strategy to Control Precise Point-to-Point Arm Movements," *Current Biology*, vol. 16, no. 8, pp. 767–772, 2006.

[11] C. R and M. A, "Elephant trunk type elastic manipulator - a tool for bulk and liquid materials transportation," *Robotica*, vol. 17, no. 1, pp. 11–16, 1999.

[12] S. Neppalli, B. Jones, W. McMahan, V. Chitrakaran, I. Walker, M. Pritts, M. Csencsits, C. Rahn, and M. Grissom, "OctArm - A soft robotic manipulator," *IEEE International Conference on Intelligent Robots and Systems*, p. 2569, 2007.

[13] J. Wu, Y. Zhao, Y. Zhang, D. Shumate, S. B. Slade, S. V. Franklin, and D. L. Hu, "Elephant trunks form joints to squeeze together small objects," *Journal of the Royal Society Interface*, vol. 15, no. 147, 2018.

[14] M. Manti, V. Cacucciolo, and M. Cianchetti, "Stiffening in soft robotics: A review of the state of the art," *IEEE Robotics and Automation Magazine*, vol. 23, no. 3, pp. 93–106, 2016.

[15] M. Zhu, Y. Mori, T. Wakayama, A. Wada, and S. Kawamura, "A Fully Multi-Material Three-Dimensional Printed Soft Gripper with Variable Stiffness for Robust Grasping," *Soft Robotics*, vol. 6, no. 4, pp. 507–519, 2019.

[16] Y. Wei, Y. Chen, T. Ren, Q. Chen, C. Yan, Y. Yang, and Y. Li, "A Novel, Variable Stiffness Robotic Gripper Based on Integrated Soft Actuating and Particle Jamming," *Soft Robotics*, vol. 3, no. 3, pp. 134–143, 2016.

[17] A. M. Nasab, A. Sabzehzar, M. Tatari, C. Majidi, and W. Shan, "A Soft Gripper with Rigidity Tunable Elastomer Strips as Ligaments," *Soft Robotics*, vol. 4, no. 4, pp. 411–420, 2017.

[18] A. Shiva, A. Stilli, Y. Noh, A. Faragasso, I. D. Falco, G. Gerboni, M. Cianchetti, A. Menciassi, K. Althoefer, and H. A. Wurdemann, "Tendon-Based Stiffening for a Pneumatically Actuated Soft Manipulator," *IEEE Robotics and Automation Letters*, vol. 1, no. 2, pp. 632–637, 2016.

[19] S. H. Ahn, K. T. Lee, H. J. Kim, R. Wu, J. S. Kim, and S. H. Song, "Smart Soft Composite: An Integrated 3D Soft Morphing Structure Using Bend-twist Coupling of Anisotropic Materials," *International Journal of Precision Engineering and Manufacturing*, vol. 13, no. 4, pp. 631–634, 2012.

[20] N. W. Bartlett, M. T. Tolley, J. T. B. Overvelde, J. C. Weaver, B. Mosadegh, K. Bertoldi, G. M. Whitesides, and R. J. Wood, "A 3d-printed, functionally graded soft robot powered by combustion," *Science*, vol. 349, no. 6244, pp. 161–165, 2015. [Online]. Available: https://science.sciencemag.org/content/349/6244/161

[21] K. Nguyen, N. Yu, M. M. Bandi, M. Venkadesan, and S. Mandre, "Curvature-induced stiffening of a fish fin," *Journal of the Royal Society Interface*, vol. 14, no. 130, 2017.

[22] V. Pini, J. J. Ruz, P. M. Kosaka, O. Malvar, M. Calleja, and J. Tamayo, "How two-dimensional bending can extraordinarily stiffen thin sheets," *Scientific Reports*, vol. 6, no. July, pp. 1–6, 2016. [Online]. Available: http://dx.doi.org/10.1038/srep29627

[23] N. P. Bende, A. A. Evans, S. Innes-Gold, L. A. Marin, I. Cohen, R. C. Hayward, and C. D. Santangelo, "Geometrically controlled snapping transitions in shells with curved creases," *Proceedings of the National Academy of Sciences of the United States of America*, vol. 112, no. 36, pp. 11 175–11 180, 2015.

[24] R. J. Webster and B. A. Jones, "Design and kinematic modeling of constant curvature continuum robots: A review," *International Journal of Robotics Research*, vol. 29, no. 13, pp. 1661–1683, 2010.

[25] H. I. Kim, M. W. Han, S. H. Song, and S. H. Ahn, "Soft morphing hand driven by SMA tendon wire," *Composites Part B: Engineering*, vol. 105, pp. 138–148, 2016. [Online]. Available: http://dx.doi.org/10.1016/j.compositesb.2016.09.004

[26] Y. Sugiyama and S. Hirai, "Crawling and jumping by a deformable robot," *International Journal of Robotics Research*, vol. 25, no. 5-6, pp. 603–620, 2006.

[27] A. B. Clark and N. Rojas, "Assessing the performance of variable stiffness continuum structures of large diameter," *IEEE Robotics and Automation Letters*, vol. 4, no. 3, pp. 2455–2462, 2019.

[28] J. Kiendl, M.-C. Hsu, M. C. Wu, and A. Reali, "Isogeometric kirchhoff–love shell formulations for general hyperelastic materials," *Computer Methods in Applied Mechanics and Engineering*, vol. 291, pp. 280 – 303, 2015. [Online]. Available: http://www.sciencedirect.com/science/article/pii/S0045782515001127

[29] A. A. Amiri Moghadam, S. Alaie, S. Deb Nath, M. Aghasizade Shaarbaf, J. K. Min, S. Dunham, and B. Mosadegh, "Laser cutting as a rapid method for fabricating thin soft pneumatic actuators and robots," *Soft Robotics*, vol. 5, no. 4, pp. 443–451, 2018.

[30] C. Tawk, M. In Het Panhuis, G. M. Spinks, and G. Alici, "Bioinspired 3d printable soft vacuum actuators for locomotion robots, grippers and artificial muscles," *Soft Robotics*, vol. 5, no. 6, pp. 685–694, 2018.

[31] UltiMaker, "Technical data sheet: TPU 95A," 2018, version 4.002. [Online]. Available: https://ultimaker.com/download/74976/UM180821%20TDS%20TPU%2095A%20RB%20V11.pdf

[32] Dynamixel, "Dynamixel XM430-W350 performance graph," 2020. [Online]. Available: http://emanual.robotis.com/docs/en/dxl/x/xm430-w350/#performance-graph